ACS APPLIED BIO MATERIALS Cite This: ACS Appl. Bio Mater. XXXX, XXX, XXX−XXX

Article

www.acsabm.org

Combined Detection of CA19−9 and MUC1 Using a Colorimetric Immunosensor Based on Magnetic Gold Nanorods for Ultrasensitive Risk Assessment of Pancreatic Cancer

Nan-Si Li,[†,‡,#] Weng-Ling Lin,[§,#] Ying-Pei Hsu,[‡] Ying-Tzu Chen,[‡] Yow-Ling Shiue,[†] and Hung-Wei Yang*[,‡]

[†]Institute of Biomedical Sciences, National Sun Yat-sen University, Kaohsiung 80424, Taiwan

[‡]Institute of Medical Science and Technology, National Sun Yat-sen University, Kaohsiung 80424, Taiwan

[§]Department of Pathology, Kaohsiung Armed Forces General Hospital, Kaohsiung 80284, Taiwan

Supporting Information

ABSTRACT: We herein report a facile approach for developing an enzyme-free colorimetric immunosensor based on a magnetic iron oxide (IO)-coated gold nanorod (MGNR) nanocomposite with high electron transfer ability to accelerate the color bleaching reaction of methyl orange (MO) in the presence of $NaBH_4$ for ultrasensitive detection of cancer antigens. In the case of MO, the reaction rate of MGNRs showed approximately 45.6-fold and 1520.8-fold higher than that of Cys-GNRs and $NaBH_4$, respectively. The proposed colorimetric immunosensor was demonstrated to enable simple, cost-effective, sensitive, and specific carbohydrate antigen 19−9 (CA19−9) and mucin 1 (MUC1) detection for risk evaluation of pancreatic cancer (PC) with a small volume of serum sample without the use of any enhancing solutions or enzymes. By increasing the concentration of CA19−9 and MUC1, more MGNRs remained in the plate well to enhance the color bleaching of MO. As a proof-of-concept, the limit of detection (LOD) of 3.5×10^{-5} U/mL for CA19−9 and 5.2×10^{-6} U/mL for MUC1 was obtained with a wide linear quantification range from 8.6×10^{-5} U/mL to 1.4×10^{-2} U/mL for CA19−9 and 1.3×10^{-5} U/mL to 2.1×10^{-3} U/mL for MUC1, suggesting potential clinical applications for the early risk evaluation of PC.

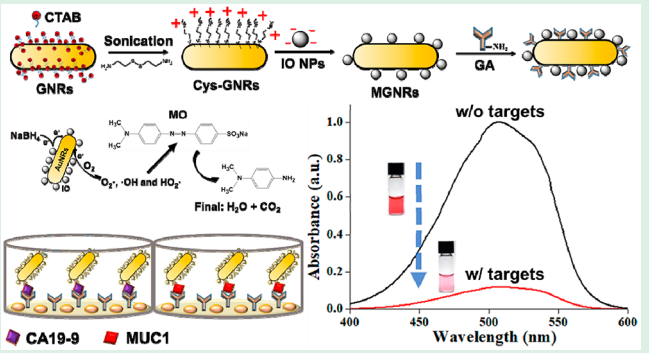

KEYWORDS: *pancreatic cancer, carbohydrate antigen 19−9 (CA19−9), mucin 1 (MUC1), enzyme-free, colorimetric biosensor*

1. INTRODUCTION

According to statistics from the American Cancer Society in 2016, the five-year survival rate of pancreatic cancer (PC) patients is less than 8%,[1] nearly the lowest among existing cancers due to the lack of early and accurate diagnostic tools. Common clinical methods for diagnosing PC are medical imaging techniques such as magnetic resonance imaging, ultrasonography, and computed tomography scan. However, it is difficult to diagnose PC at an early stage by these medical imaging systems, resulting in the failure of standard clinical treatment. Therefore, it is urgent to develop a biosensor with rapid, simple, cheap, and accurate detection methods for the specific biomarker in an early PC diagnosis.

The cancer marker carbohydrate antigen 19−9 (CA19−9) is one of the most important tumor biomarkers in patients with gastrointestinal malignancies, and also frequently found in PC patients, with a high score of over 79%.[2] Moreover, some patients may receive a false-positive diagnosis for PC because of pancreatitis, cirrhosis, and bile duct diseases, which can all increase CA19−9 levels. Mucin 1 (MUC1), a cell surface associated protein, is another potential epithelial tumor biomarker that is also dramatically overexpressed in early PC.[3,4] The level of MUC1 in serum is associated with the development and metastasis of PC.[5] Therefore, MUC1 may be a suitable candidate as a biomarker for enhancing the accuracy and selectivity of a PC diagnosis with CA19−9.

Thus, far, some colorimetric immunosensors have been developed for detection of CA19−9 or MUC1, including enzyme-linked immunosorbent assay (ELISA),[6] electrochemiluminescence (ECL),[7−9] etc. However, the expensive enzyme used to catalyze H_2O_2 to oxidize substrates (i.e., 3,3′,5,5′-tetramethylbenzidine (TMB)) for producing signals, horseradish peroxidase (HRP), is environmentally unstable, and the substrates must be stored in a dark and cold room. Therefore, the synthesis of a stable and cheap catalyzer to decolorize an easy-to-store substrate has the potential to take advantage of

Received: July 8, 2019
Accepted: September 26, 2019
Published: September 26, 2019

DOI: 10.1021/acsabm.9b00616
ACS Appl. Bio Mater. XXXX, XXX, XXX−XXX

new colorimetric biosensor development. Methyl orange (MO) is a common, stable, and cheap acid−base indicator. It could be easily mineralized with gold nanoparticles so that its color would be decolorized and decrease in its unique optical absorbance at 460 nm,[10] which means MO could be a possible signal source in the biosensing field.

Herein, we demonstrated an ultrasensitive colorimetric immunosensor based on the decolorization of MO by prepared magnetic iron oxide (IO)-coated gold nanorods (MGNRs) with high electron transfer ability to accelerate the catalysis rate in the presence of $NaBH_4$ or evaluation of the level of CA19−9 and MUC1, with just a small volume of serum sample required. Based on these studies, a novel, simple, timesaving, stable, and sensitive biosensor to detect CA19−9 and MUC1 would be more outstanding. This decolorization examination approach can potentially offer a tool with rapid detection and high accuracy compared with current tests and is based on immunological mechanisms.

2. EXPERIMENTAL METHODS

2.1. Materials. Bovine serum albumin (BSA), cetyltrimethylammonium bromide (CTAB), cystamine dihydrochloride, glutaraldehyde (GA), hexylamine, hydrogen tetrachlorocuprate trihydrate, iron(II) chloride tetrahydrate ($FeCl_2{\cdot}4H_2O$), iron(III) chloride hexahydrate ($FeCl_3{\cdot}6H_2O$), L-ascorbic acid (AA), 4-dimethylaminoazobenzene-4′-sulfonic acid sodium salt (Methyl Orange), silver nitrate ($AgNO_3$), sodium borohydride ($NaBH_4$), and sodium hydroxide (NaOH) were purchased from Sigma-Aldrich (St. Louis, MO, USA). Anti-human CA19−9 rabbit monoclonal antibody ($CA19{-}9_{Ab}$) and anti-human MUC1 mouse monoclonal antibody ($MUC1_{Ab}$) were obtained from MyBioSource (USA) and GeneTex (USA), respectively. Human CA19−9 antigen was purchased from Cloud-clone, USA, and human MUC1 antigen was obtained from Sino Biological, CN. Human CA19−9 ELISA kit and human MUC1 ELISA kit were obtained from Elabscience, CN. Pierce BCA Protein Assay Kit was obtained from Thermo Scientific, USA. Goat anti-mouse IgG-HRP and goat anti-rabbit IgG-HRP were all purchased from LeadGENE, Taiwan. Luminata Crescendo Western HRP Substrate was obtained from Millipore, USA.

2.2. Apparatus. Luminescence detections were performed by the microtiter plate reader (SpectraMax M2; Molecular Devices Co., California, USA), and the hysteresis curve was obtained from SQUID (MPMS XL-7, Quantum Design INC., USA). The absorbance spectrum and the ζ potential of materials were detected with UV/vis/NIR spectrometers (MODEL V-700, JASCO, Japan) and dynamic light scattering (DLS, SZ-100, HORIBA, Japan). The IR spectrum was measured with a Fourier transform infrared spectrometer (FTIR, T-27, BRUKER, USA). The morphology of MGNRs was characterized by transmission electron microscopy (TEM, H-7500, Hitachi) and scanning electron microscopy (SEM, SU8220, Hitachi).

2.3. Preparation of Amino Functionalized Gold Nanorods (Cys-GNRs). The CTAB-capping gold nanorods (GNRs) were prepared based on a slight change to the previously reported method.[11] Briefly, the seed solution was first prepared by adding 0.2 mL of 0.01 M $HAuCl_4$ in 7.5 mL of aqueous 0.1 M CTAB, followed by immediately adding 0.6 mL of ice-cold $NaBH_4$ (0.01 M), resulting in a color change of the solution from yellow to brownish-yellow. The seed solution was aged at room temperature for at least 2 h for further application. For preparing the GNRs, 50 μL of the prepared seed solution was quickly added to the growth solution (9.5 mL of 0.1 M CTAB + 0.4 mL of 0.01 M $HAuCl_4$ + 25 μL of 0.01 M $AgNO_3$ + 64 μL of 0.1 M AA) with sufficient oscillation for 20 s. The solutions were incubated in a water bath for at least 12 h with the temperature maintained at 28 °C to ensure the full growth of GNRs. The excessive CTAB on the surface of GNRs and in the supernatant was removed by centrifugation (12 000 rpm for 20 min), and the obtained GNRs solution was stored in a 20 mL brown glass bottle at 4 °C to extend the shelf life.

According to a previous study,[12] the prepared GNRs were mixed with 1 mL of 200 mM cystamine dihydrochloride under vigorous sonication at 50 °C for 3 h to obtain Cys-GNRs. Subsequently, the Cys-GNRs were obtained by washing with deionized water (DI-H_2O) three times to remove excessive cystamine dihydrochloride. Finally, the Cys-GNRs were redispersed in 10 mL of DI-H_2O and stored at room temperature for further use.

2.4. Preparation of MGNRs. Detailed synthesis procedures of high-magnetization iron oxide nanoparticles (IO NPs) with negative charge were previously reported.[13−15] First, 10 mL of prepared Cys-GNRs with a positive charge were mixed with 100 μL of IO NPs by gentle vortexing and incubated at room temperature for 30 min to obtain MGNRs. Complexes were washed with DI-H_2O to remove unreacted Cys-GNRs and then dispersed in 1 mL of DI-H_2O.

2.5. Preparation of Antibody-Conjugated MGNRs. For the conjugation of antibodies ($CA19{-}9_{Ab}$ or $MUC1_{Ab}$) on the MGNRs, the GA was used as a link to connect the amine groups (NH_2) between the MGNRs and antibodies. Briefly, 100 μL of MGNRs and 100 μL of antibodies (1 ng/μL $CA19{-}9_{Ab}$ or $MUC1_{Ab}$ in tris-buffered saline (TBS, pH 7.4) solution) were mixed, first for 30 min. Then 50 μL different concentrations (0.1, 0.5, 1, 2,5, 5 wt %) of GA solution were added and allowed to react uniformly for another 3 h at room temperature in the dark. After being washed with DI-H_2O to remove unreacted GA and antibodies with a magnet, the obtained $CA19{-}9_{Ab}$-conjugated MGNRs ($MGNRs_{CA19-9}$) or $MUC1_{Ab}$-conjugated MGNRs ($MGNRs_{MUC1}$) were dispersed in 100 μL TBS. To prevent nonspecific binding with other proteins, the $MGNRs_{CA19-9}$ or $MGNRs_{MUC1}$ were mixed with 100 μL aqueous hexylamine (1 mg/mL) for 1 h at room temperature to block the residual activity of GA, then washed with DI-H_2O to remove excess hexylamine with a magnet and redispersed in 100 μL TBS. The successful conjugation of $CA19{-}9_{Ab}$ or $MUC1_{Ab}$ on the MGNRs was investigated by measuring the chemiluminescence intensity using an HRP-labeled secondary antibody and Luminata Crescendo Western HRP Substrate.

2.6. Preparation of Sensing Wells with Antibody Coating. The $CA19{-}9_{Ab}$ or $MUC1_{Ab}$ was diluted to 2 μg/mL in a carbonate-bicarbonate buffer (CBS) solution (0.05 M Na_2CO_3, 0.05 M $NaHCO_3$, pH 9.6), and 100 μL of the solution was added into each well of a 96-well plate. After incubation overnight at 4 °C, the wells were washed three times with 300 μL tris-buffered saline with Tween 20 (TBST), then blocked with blocking buffer (2% BSA in TBST) at room temperature for 1 h. After that, each well was washed three times with 300 μL TBST to obtain antibody-coated wells. The capacity of $CA19{-}9_{Ab}$ or $MUC1_{Ab}$ immobilized on the well of 96-well plate was calculated by measuring the chemiluminescence intensity using HRP-labeled secondary antibody and Luminata Crescendo Western HRP Substrate.

2.7. Colorimetric Assay for CA19−9 and MUC1 Detection. The CA19−9 and MUC1 were diluted to 0.05, 0.25, 1, 2, 4, and 8 ng/mL with sample dilution buffer (0.1% BSA in TBST), then 100 μL of each concentrations of CA19−9 or MUC1 and 100 μL of $MGNRs_{CA19-9}$/$MGNRs_{MUC1}$ mixture was together added to each well, incubating at room temperature for 30 min then washed three times with 100 μL TBST. Next, 100 μL of MO and 100 μL of 5% $NaBH_4$ were added into each well, and the plate was placed at 37 °C for 10 min. The reaction was then terminated by adding 10 μL of 1 M H_2SO_4, followed by absorbance intensity measurement at 508 nm (A_{508nm}) using a microplate reader (SpectraMax M2). The A_{508nm} was linearly proportional to the concentration of CA19−9 and MUC1.

2.8. Interference Tests. We utilized interference experiments to verify that our immunosensor has good selectivity and specificity. Various substances, such as urea (UA, 0.3 mM), ascorbic acid (AA; 4.3 μg/mL), bovine serum albumin (BSA; 1 mg/mL), fetal bovine serum (FBS, 10%), IgG (100 μg/mL), carcinoembryonic antigen (CEA, 100 ng/mL), vascular endothelial growth factor (VEGF, 100 ng/mL), FXYD domain-containing ion transport regulator 3 (FXYD3, 100 ng/mL), CA19−9 (5 ng/mL), and MUC1 (5 ng/mL) were employed.

DOI: 10.1021/acsabm.9b00616
ACS Appl. Bio Mater. XXXX, XXX, XXX−XXX

Scheme 1. Illustration of the Preparation Process for $MGNRs_{CA19-9}$, $MGNRs_{MUC1}$, Colorimetric Immunosensor, and the Detection Procedures of CA19-9 and MUC1 Based on the Decolorization of MO by MGNRs in the Presence of $NaBH_4$

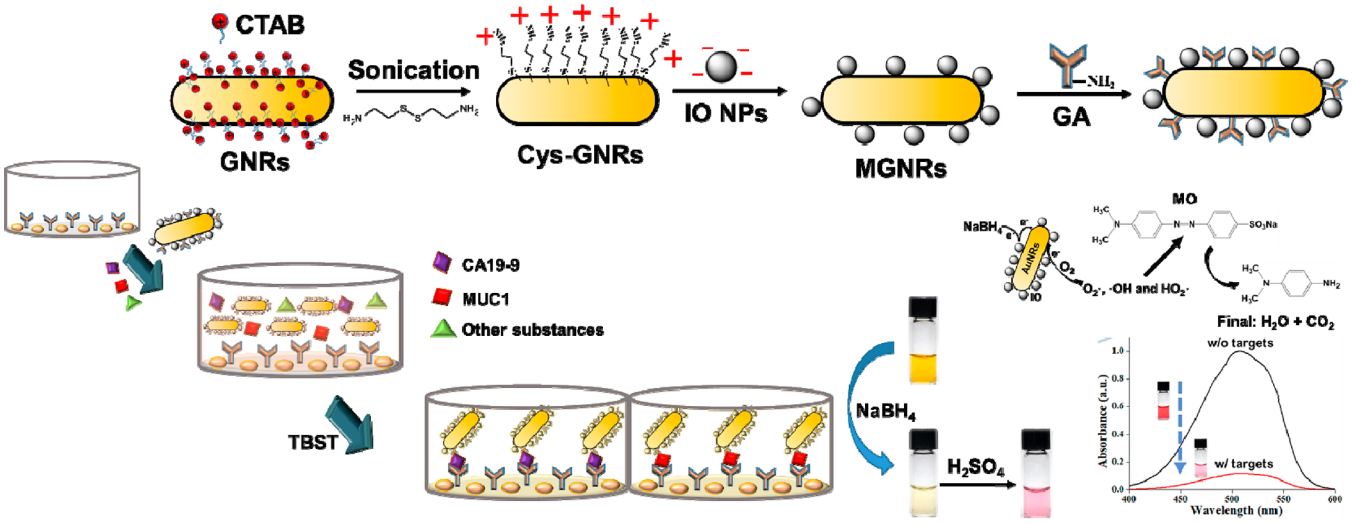

First, 100 μL of the interferences, CA19−9 or MUC1, and 100 μL of the $MGNRs_{CA19-9}$/$MGNRs_{MUC1}$ mixture were added to each well together, incubating at room temperature for 30 min then washed three times with 100 μL TBST. Next, 100 μL of MO and 100 μL of 5% $NaBH_4$ were added into each well, and the plate was placed at 37 °C for 10 min. The reaction was then terminated by adding 10 μL of 1 M H_2SO_4, followed by an absorbance intensity measurement at 508 nm (A_{508nm}) using a microplate reader (SpectraMax M2) to determine the ability of anti-interference.

2.9. Recovery Studies of CA19−9 and MUC1 in Normal Serum. Approximately 1 mL of human blood from a healthy donor was collected with a lithium heparin tube as an anticoagulant agent. The collected blood was immediately centrifuged (3000 rpm) at 4 °C for 15 min. The obtained serum was diluted for 10^5-fold and spiked with various concentrations of CA19−9 or MUC1 proteins for recovery tests. Briefly, one hundred microliter of diluted serum solution was spiked with different concentrations of CA19−9 or MUC1 from 0.75 ng/mL (1.296×10^{-3} U/mL for CA19−9; 1.935×10^{-4} U/mL for MUC1) to 5 ng/mL (8.640×10^{-3} U/mL for CA19−9; 1.290×10^{-3} U/mL for MUC1) and 100 μL of $MGNRs_{CA19-9}$/$MGNRs_{MUC1}$ mixture was added to sensing wells with antibody-coating and incubated for 30 min at room temperature; the sensing wells were washed three times with TBST, developing through the addition of 100 μL of MO and 100 μL of 5% $NaBH_4$ at 37 °C for another 10 min and then stopped by the addition of 10 μL of 1 M H_2SO_4. The A_{508nm} was recorded and calculated for ΔA_{508nm} to determine the CA19−9 or MUC1 concentration in serum using the microplate reader (SpectraMax M2) to evaluate the recovery rate.

2.10. Statistical Analysis. The data were expressed as mean ± SD on the basis of at least three independent experiments (three independent experiments for antibody conjugation analysis in Figure 3 and recovery studies; six independent experiments for others). Statistical analysis was performed using a Student's t test; $^*p < 0.05$ and $^{**}p \leq 0.001$ were considered statistically significant.

3. RESULTS AND DISCUSSION

3.1. Synthesis and Characterizations of MGNRs. The scheme of the MGNRs synthesis and the biosensing mechanism of targets (CA19−9 and MUC1) is shown in Scheme 1. The GNRs were first modified with cystamine to for Cys-GNRs with positive charge and rich amine groups on the surface then mixed with negatively charged IO NPs to form MGNRs. The $CA19-9_{Ab}$ or $MUC1_{Ab}$ were further conjugated on the MGNRs with a GA linker to form $MGNRs_{CA19-9}$ or $MGNRs_{MUC1}$ as a decolorization probe. We hypothesized that each captured target protein (CA19−9 or MUC1) would allow for the retention of large amounts of $MGNRs_{CA19-9}$ or $MGNRs_{MUC1}$, thereby initiating the catalytic reduction of MO in the presence of $NaBH_4$ to decrease its absorbance intensity at 464 nm (A_{464nm}), then stop the reaction by adding H_2SO_4 to record the change of absorbance intensity at 508 nm (A_{508nm}) for ultrasensitive detection of CA19−9 and MUC1 in early PC diagnosis.

The successful fabrication of MGNRs was confirmed by the ζ potential, which changed to +28.9 ± 1.8 mV (Cys-GNRs) from +56.5 ± 2.4 mV (GNRs), then further decreased to +12.3 ± 4.5 mV (MGNRs). This change indicated the successful surface ligand exchange to cystamine from CTAB by Au−S bond and absorption of negatively charged IO NPs on the Cys-GNRs surface (Supporting Information Figure S1). Furthermore, the GNRs displayed a weak transverse plasmon (TP) band at 510 nm and a strong longitudinal plasmon (LP) band at 865 nm. After cystamine modification, there was a redshift in the LP band to 892 nm from 865, most likely because the double CTAB layer was replaced with small thio-molecules (i.e., cystamine) leading to the LP change in refractive index (RI). Additionally, the baseline of absorption was changed, and showing a shoulder peak at approximately 350−400 nm after the IO NPs attachment (Figure 1A).[14,15] Note that the longitudinal band was blue-shifted to 880 nm after IO NPs attachment on Cys-GNRs from 892 nm, most likely because the IO attachment affected the aspect ratio to cause LP change in RI of Cys-GNRs, also confirmed the formation of the MGNRs hybrid structure.[16,17]

The FTIR spectrum of the IO NPs represented a peak at 576 cm^{-1} correspond to the Fe—O stretching vibration of Fe_3O_4.[18] After adsorbed on Cys-GNRs to form MGNRs, the FTIR spectrum exhibited additional bands consistent with the main vibration modes of cystamine and GNRs; the peaks at 2850 and 2918 cm^{-1} were assigned to the stretching vibration of C—CH_2 of CTAB,[19] the peak at 2918 cm^{-1} was due to the presence of the C═N and C—N bond in cysteamine,[20] and the prominent peak at 1632 cm^{-1} was due to the gold nanoparticles in both colloids (Figure 1B).[21] The average length and width of Cys-GNRs were measured as 41.2 ± 4.4 and 10.1 ± 0.9 nm, respectively (about 4.1:1 aspect ratio), by

DOI: 10.1021/acsabm.9b00616
ACS Appl. Bio Mater. XXXX, XXX, XXX−XXX

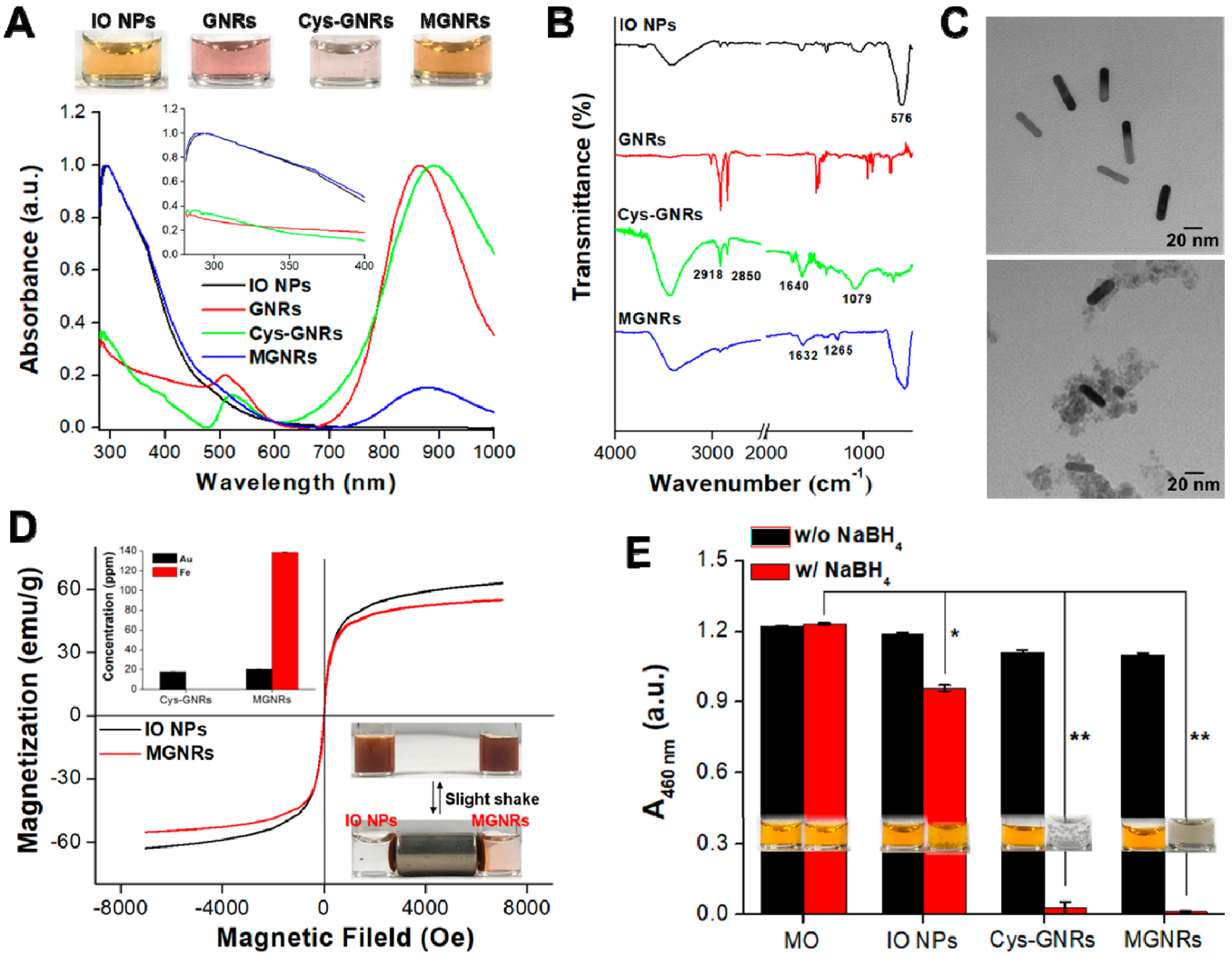

Figure 1. (A) The corresponding UV−vis spectra of the IO NPs, GNRs, Cys-GNRs, and MGNRs solutions; the inset is a digital photo of the above solutions. (B) The FTIR spectra of IO NPs, GNRs, Cys-GNRs, and MGNRs. (C) TEM images of Cys-GNRs (top) and MGNRs (bottom). (D) The magnetic hysteresis curves of IO NPs and MGNRs at room temperature; the insets are the elemental analysis by ICP-OES (top left) and a digital photo of the IO NPs and MGNRs suspensions with and without an exterior magnetic field (bottom right). (E) Comparison of the catalytic activity of IO NPs, Cys-GNRs, and MGNRs for reduction of MOs in the absence or presence of $NaBH_4$ ($n = 6$). Asterisk indicates a significant difference compared PBS (Student's t test, $^*p \leq 0.05$, $^{**}p \leq 0.001$).

TEM, with the obvious capping of IO NPs on the surface of Cys-GNRs observed by electrostatic adsorption after mixing Cys-GNRs with IO NPs (Figure 1C). Upon adsorption of the IO NPs to form MGNRs, the magnetization increased from 0 to 55.1 emu/g with superparamagnetic behavior measured by the Superconducting Quantum Interference Device (SQUID). This result was lower than the magnetization of pure IO NPs (63.2 emu/g) due to the decrease of IO NPs (12.7%) and increase of Cys-GNRs (13.1%) per unit weight of MGNRs measured by inductively coupled plasma-optical emission spectrometry (ICP-OES), but it was still sufficient to mediate magnetic attraction and catalysis (Figure 1D).

3.2. Catalytic Efficiency of MGNRs. To demonstrate the principle mentioned above, we first investigated the catalytic capability of MGNRs to decolorize MO in the presence of $NaBH_4$, which is shown in Figure 1E. The decolorization of MO could not be proceeded even with excessive $NaBH_4$ in the absence of GNRs catalyst, as evidenced by determining the color change (Figure 1E, inset) and the change of A_{460nm} of MO.[22] The results demonstrated that the IO NPs exhibited little catalytic activity to reduce the MO in the presence of $NaBH_4$, but the efficiency is far less than Cys-GNRs and MGNRs. To understand the catalytic efficiency between Cys-GNRs and MGNRs, the kinetic reactions were assayed by reacting Cys-GNRs or MGNRs with different concentrations of MO in the presence of constant $NaBH_4$ (Figure 2A). The required time for the complete reduction of MO increased as the MO concentration increased in both Cys-GNRs and MGNRs groups.

Interestingly, the reduction rate of MGNRs toward MO was much faster than that of Cys-GNRs; for example, only 41 s was required to completely reduce 125 μM of MO with MGNRs, but the required time must increase to 576 s to completely reduce the same concentration of MO by Cys-GNRs. This difference is most likely because the IO NPs can help the electrons transfer between Au and BH_4^-, and it also provides an alternate step to reduce the activation energy among MO, Au, and $NaBH_4$.[23] It could limit the distance of each compound in each nanoparticle by larger surface area, space barriers, and intermolecular force so that it could accelerate the

DOI: 10.1021/acsabm.9b00616
ACS Appl. Bio Mater. XXXX, XXX, XXX−XXX

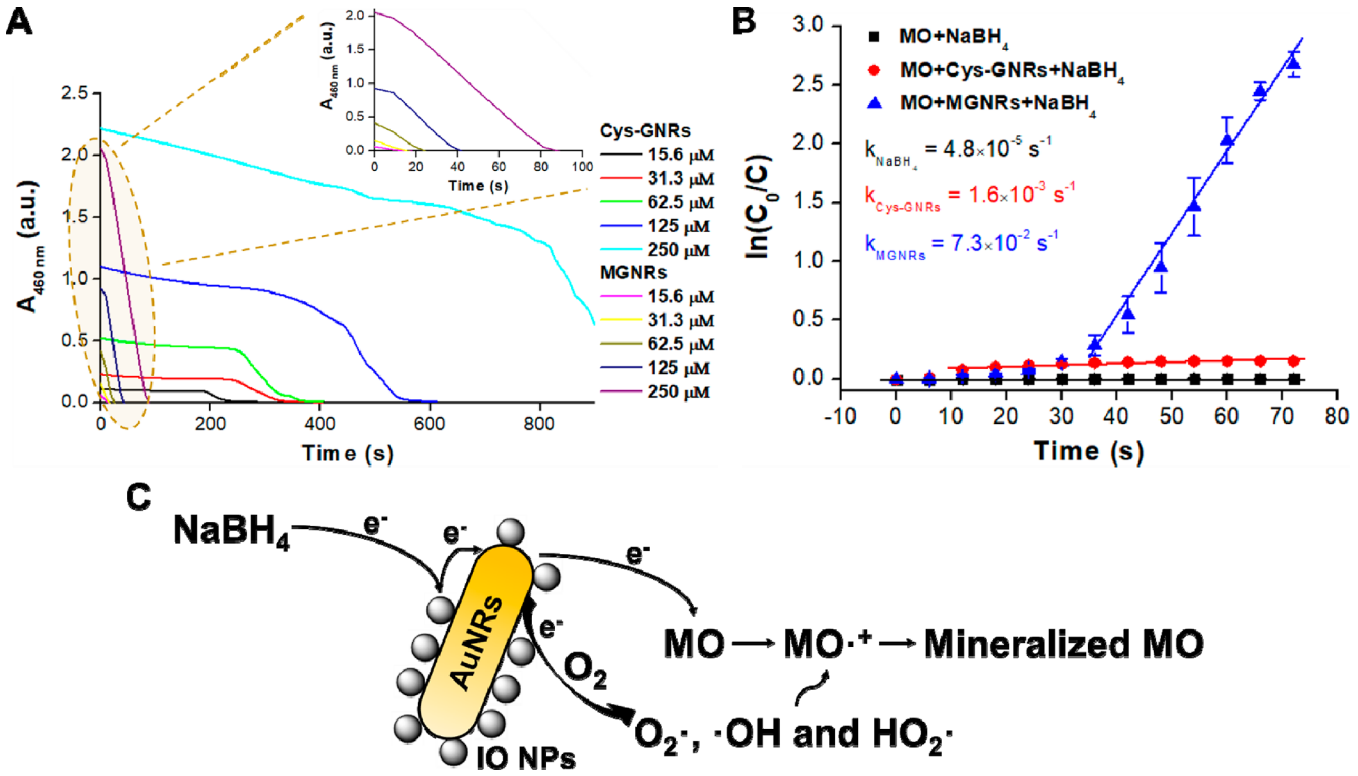

Figure 2. (A) The kinetics of a complete catalytic reduction of different MO concentrations by $NaBH_4$ in the presence of a constant concentration of Cys-GNRs and MGNRs. (B) The kinetics of catalytic reduction of MO by $NaBH_4$ in the presence of Cys-GNRs and MGNRs. The graph was fitted with linearity from which rate constants were determined (n = 6). (C) Proposed mechanism of the MO catalytic reduction of MO into respective end products in the presence of the MGNRs nanocomplexes. O_2 is the adsorbed oxygen on IO NPs surface which leads to the formation of $O_2^{\bullet}$, $^{\bullet}OH$, and $HO_2^{\bullet}$.

rate of electron transfer. To confirm that, we quantified the catalytic efficiency of MGNRs by calculating the respective first-order rate constants (k). The first-order Langmuir–Hinshelwood kinetic equation is presented:

$$\ln\left(\frac{C_0}{C}\right) = \ln\left(\frac{A_0}{A}\right) = kt$$

where C_0 and C are the initial concentration and reaction concentration at time t of MO, respectively; A_0 and A are the initial A_{460nm} and the A_{460nm} at time t of MO, respectively.

According to the Beer's law, $A = \alpha \times l \times C$, where A is absorbance, α is absorption coefficient, l is the length of the optical path, and C is the concentration. The $\alpha \times l$ are same when the A_{460nm} measured by the same types of cuvettes, originates from the same indicator (MO), resulting in A and C are directly proportional.

Figure 2B shows a plot of $\ln(C_0/C)$ vs time for the catalytic reduction of MO by $NaBH_4$ only, Cys-GNRs+$NaBH_4$, and MGNRs+$NaBH_4$. The linear regression plots fit well, and the slopes of each plot were calculated and used to obtain the k. The k for MO reduction was found to be $k_{NaBH_4} = 4.8 \times 10^{-5}$ s^{-1}, $k_{Cys\text{-}GNRs} = 1.6 \times 10^{-3}$ s^{-1}, and $k_{MGNRs} = 7.3 \times 10^{-2}$ s^{-1}. The higher k value, the faster reduction rate of MO, thus the superior catalytic activity of the MGNRs compared with pure GNRs and Au-TiO_2.[10] In the case of MO, the reaction rate of MGNRs showed approximately 45.6- and 1520.8-fold higher than that of Cys-GNRs and $NaBH_4$, respectively. This phenomenon can possibly be attributed to the peroxidase-like activity of IO NPs,[24] which first transfers the electrons from $NaBH_4$ to form radicals (i.e., $O_2^{\bullet}$, $^{\bullet}OH$, and $HO_2^{\bullet}$) immediately then mineralized MO (Figure 2C). Therefore, there is no obvious degradation of MO in the earlier 36 s. After that, enough radicals start to transfer the electrons by the MGNRs to rapidly mineralize MO to its end products with no color via the following reactions:[25]

$$MO + n\bar{e} + nH^+ \rightarrow \text{protonated and reduced } MO^+$$

$$MO^{\bullet+} + HO \rightarrow MO + {}^{\bullet}OH$$

$$MO + 2{}^{\bullet}OH \rightarrow H_2O + \text{oxidation products}$$

$$MO^{\bullet+} + O_2^{\bullet} \rightarrow DO_2 \rightarrow \text{mineralized products}$$

$$MO^{\bullet+} + 2HO_2^{\bullet}\ (\text{or}\ {}^{\bullet}OH) \rightarrow DO_2 \rightarrow \text{mineralized products}$$

The results demonstrated that the MGNRs exhibited a faster catalytic rate than Cys-GNRs to decrease the detection time requirement and increase the sensitivity significantly.

According to a previous study, the absorbance intensity at 508 nm for the acidic form (red color) of MO has an approximate 1.7-fold increase above that of its corresponding basic form (yellow color) at 464 nm while maintaining them at equal concentrations, most likely because of the increase in molar extinction coefficient according to the Beer–Lambert absorption law.[26] Therefore, in this study, an H_2SO_4 (1 M) solution was utilized to terminate the MGNRs-catalyzed decolorization reaction of MO by neutralizing the excessive $NaBH_4$ to terminate the reaction and amplify 1.7-fold absorbance intensity to enhance the sensing sensitivity (Figure S2). The absorbance intensity at 508 nm (A_{508nm}) was

DOI: 10.1021/acsabm.9b00616
ACS Appl. Bio Mater. XXXX, XXX, XXX–XXX

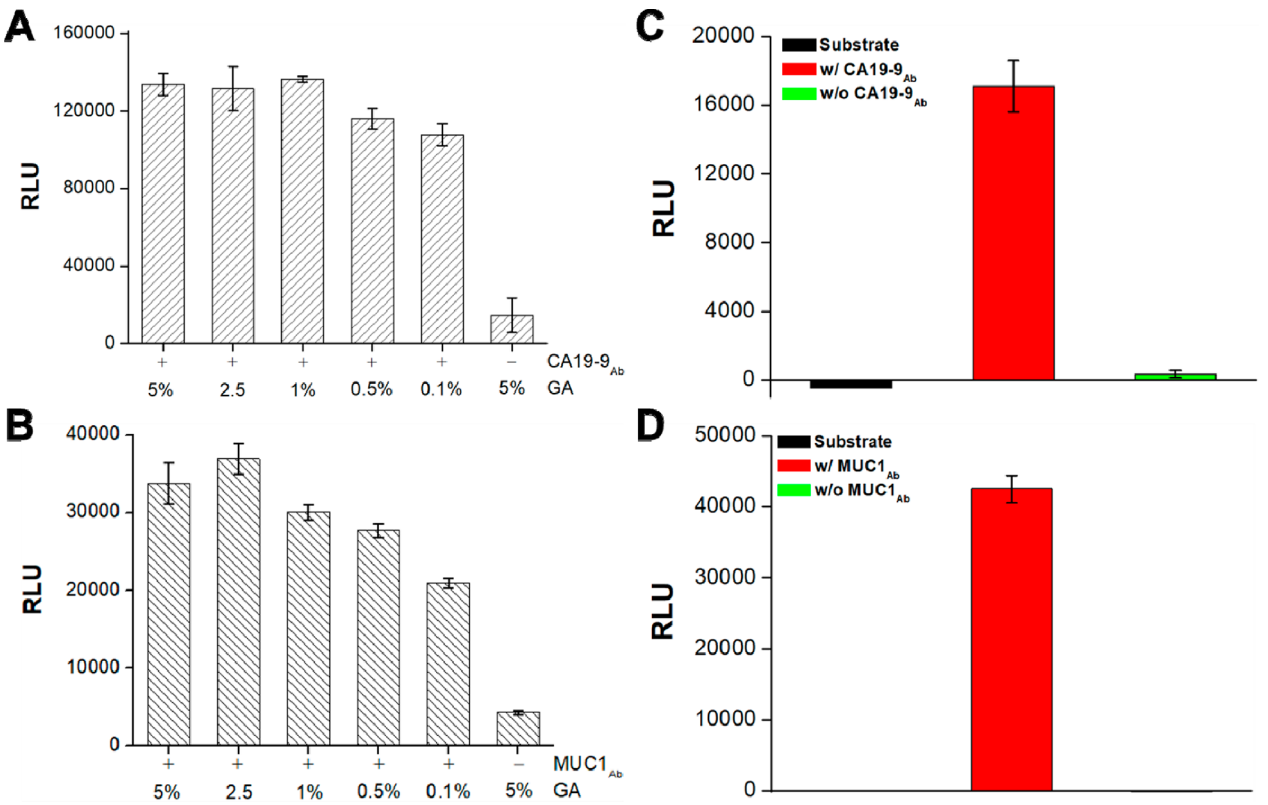

Figure 3. (A) Analysis of the optimal conjugation rate of CA19−9$_{Ab}$ on MGNRs using different GA concentrations by chemiluminescence assay (n = 3). (B) Analysis of the optimal conjugation rate of MUC1$_{Ab}$ on MGNRs using different GA concentrations with chemiluminescence assay (n = 3). (C) Confirmation of successful CA19−9$_{Ab}$ coating on plate well using chemiluminescence assay (n = 3). (D) Confirmation of successful MUC1$_{Ab}$ coating on plate well using chemiluminescence assay (n = 3).

recorded to determine the concentration of captured target proteins.

3.3. Stability Study of MGNRs. The deficiency of stability is the most general and critical problem of enzymatic biosensors because the enzymes are easily denatured in an aqueous environment. Thus, we examined the stability of MGNRs after storing for different periods (1−90 days) at 25, 37, and 50 °C; a constant MO concentration was reacted with the MGNRs stored at each time point in the presence of fresh $NaBH_4$ to determine the catalytic activity. As seen in Supporting Information Figure S3, the MGNRs were used to catalyze the reduction of MO in the presence of $NaBH_4$ without any activity decay when stored at 25 and 37 °C for 90 days. Notably, the MGNRs can maintain entire catalytic activity without any decay after storage for 90 days at 50 °C. The results indicated that MGNRs are more suitable than natural enzymes as a catalyst in dye-reduction-based (i.e., MO) decolorization analysis in any detection environments.

3.4. Antibodies Conjugation on MGNRs and Plate Wells. To make the decolorization-based biosensing system, the MGNRs and plate wells must be modified with CA19−9$_{Ab}$ and MUC1$_{Ab}$, respectively. Subsequently, we analyzed the number of antibodies on the MGNRs and plate wells after the modification process to prove the successful modification of CA19−9$_{Ab}$ or MUC1$_{Ab}$ on MGNRs and plate wells by luminescence staining. We first determined if the concentration of GA cross-linking reagent affected the immobilization efficacy of CA19−9$_{Ab}$ and MUC1$_{Ab}$, the CA19−9$_{Ab}$ and MUC1$_{Ab}$ concentration on the MGNRs. The results showed that strong luminescence was observed after CA19−9$_{Ab}$ immobilized on MGNRs with GA compared with control (without GA addition), the luminescence intensity reached saturation when the GA concentration was higher than 1% (w/v) (Figure 3A). Similar results were observed in the group of MUC1$_{Ab}$ immobilization on MGNRs with GA, but the luminescence intensity reached saturation when the concentration of GA cross-linking reagent was higher than 2.5% (w/v) (Figure 3B). The results confirmed that the CA19−9$_{Ab}$ and MUC1$_{Ab}$ were indeed successfully immobilized on MGNRs and 2.5% (w/v) of GA was the best parameter for antibody immobilization.

To ensure the successful coating of antibodies on the plate well bottom and no nonspecific adsorption, the wells were incubated with 200 μL HRP-labeled anti-rabbit secondary antibody (for CA19−9$_{Ab}$) or HRP-labeled anti-mouse secondary antibody (for MUC1$_{Ab}$) after BSA blocking (Figure 3C,D). The results demonstrated no significant luminescence exhibition in wells (substrate only and BSA blocking + substrate) for both CA19−9$_{Ab}$ and MUC1$_{Ab}$ staining. Conversely, strong luminescence was observed in the wells coated with CA19−9$_{Ab}$ or MUC1$_{Ab}$, indicating the successful coating of antibodies on the well bottom and no nonspecific adsorption effect, which can be used for CA19−9, MUC1 capture and detection.

3.5. Colorimetric Immunoassay of CA19−9 and MUC1 Proteins. The combination of CA-19−9 and MUC1 detection would be helpful for a more accurate early diagnosis of PC. The blood levels of CA19−9 and MUC1 in patients with PC is much higher than in healthy people (cutoff concentration: 37.0 U/mL for CA19−9, 10.2 U/mL for MUC1), indicating its

DOI: 10.1021/acsabm.9b00616
ACS Appl. Bio Mater. XXXX, XXX, XXX−XXX

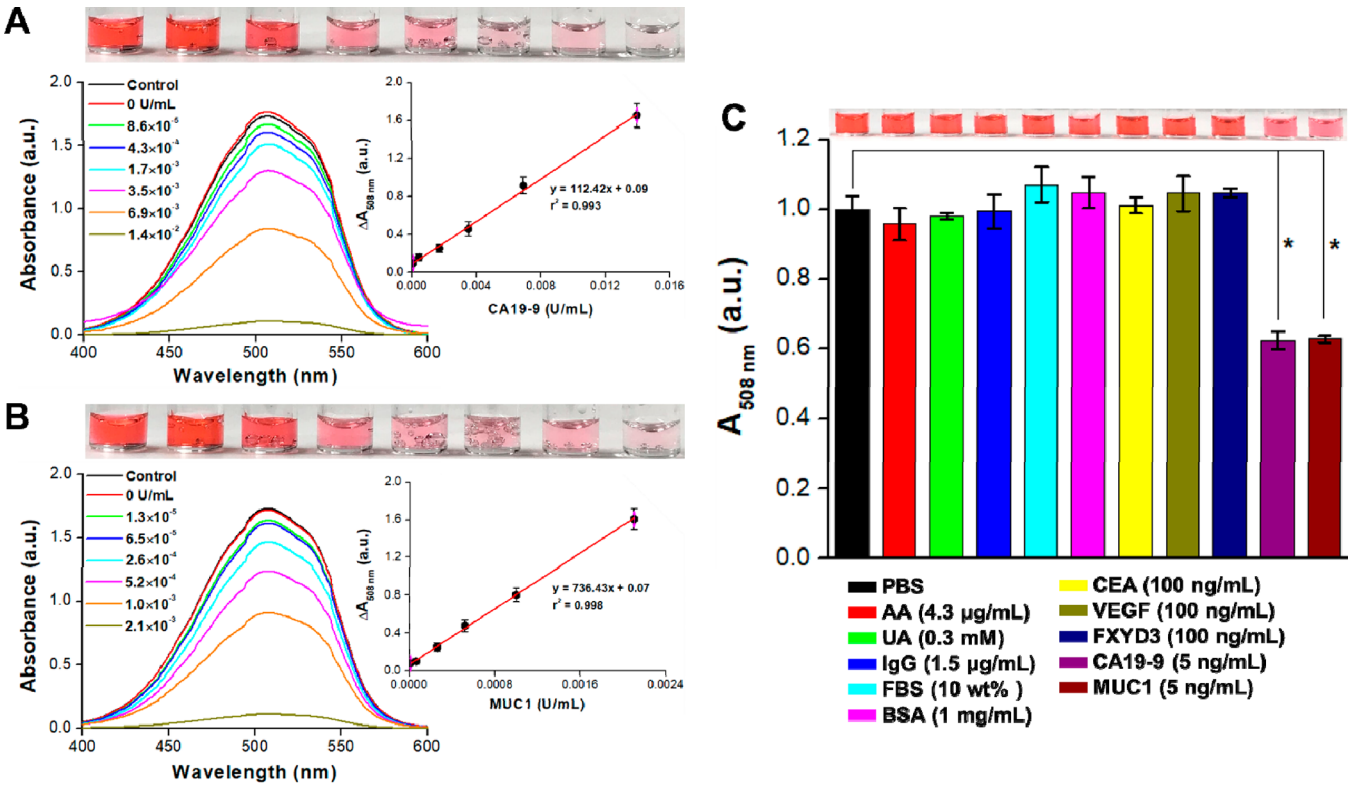

Figure 4. (A) The typical UV−vis absorption spectra of the MO solution in the presence of CA19−9 at various concentrations using $MGNRs_{CA19-9}/MGNRs_{MUC1}$ as the catalyst; insets are the linear calibration curve between the ΔA_{508nm} against the concentration of CA19−9 (n = 6) and the corresponding digital photos. (B) Typical UV−vis absorption spectra of the MO solution in the presence of MUC1 at various concentrations using $MGNRs_{CA19-9}/MGNRs_{MUC1}$ as the catalyst. Insets are the linear calibration curve between the ΔA_{508nm} against the concentration of MUC1 (n = 6) and the corresponding digital photos. (C) Specificity test of catalytic MGNRs-based colorimetric immunosensing for CA19−9 and MUC1 (n = 6); inset is the corresponding digital photos. Asterisk indicates a significant difference compared PBS (Student's t test, $^*p \leq 0.05$).

potentiality in developing trustworthy PC diagnosis and prognosis monitoring.[27,28] Because the clinical serum samples from PC patients are fairly precious, the detection range and LOD must be as low as possible to allow multiple dilutions of the samples. The absorbance of MO decreased with the concentration of CA19−9 or MUC1 increase, indicating that more MGNRs would be bound on the wells to reduce MO in the presence of more CA19−9 and MUC1. First, we determined that 100 μg/mL standard of CA19−9 and MUC1 are equal to 18.58 U/mL and 25.8 U/mL by commercial ELISA kits and the BCA protein kit. The standard curve was linear and in the range of 8.6×10^{-5} U/mL to 1.4×10^{-2} U/mL for CA19−9 with a LOD of 3.5×10^{-5} U/mL (r^2 = 0.991) and 1.3×10^{-5} U/mL to 2.1×10^{-3} U/mL for MUC1 with a LOD of 5.2×10^{-6} U/mL (r^2 = 0.996) using MGNRs as the catalyst to decolorize MO in the presence $NaBH_4$ (Figure 4A,B).

The detection range and LOD sufficiently determined the suffering risk of PC and allowed at least 10^5-fold dilution of the original serum sample for analysis. We also compared the performance of numerous optical biosensing systems for CA19−9 and MUC1 with our decolorization sensing system (Table 1 and Table 2). The results mentioned above demonstrated that this proposed colorimetric biosensing system based on the reduction of MO by MGNRs with high catalytic activity in the presence of $NaBH_4$ worked well, and this approach may offer a more accurate and faster alternative compared with current tests do for early PC diagnosis and prognosis monitoring.

Table 1. Comparison of Our Present Work with Other Methods for CA19-9 Immunosensing

measurement method	linear range (U/mL)	detection limit (U/mL)
electrochemical immunoassay[29]	10^{-3} to 12	5×10^{-4}
fluorescence immunoassay[30]	10^{-6} to 1	7.7×10^{-7}
electrochemiluminescence[31]	5×10^{-4} to 1.5×10^{2}	2×10^{-4}
decolorization immunoassay (this work)	8.6×10^{-5} to 1.4×10^{-2}	3.5×10^{-5}

Table 2. Comparison of Our Present Work with Other Methods for MUC1 Immunosensing

measurement method	linear range	detection limit
electrochemical immunoassay[32]	8.8−353.3 nM	2.2 nM
fluorescence immunoassay[33]	4×10^4 to 10^7 nM	28 nM
electrochemiluminescence[34]	10^{-2} to 10^4 pg/mL	4.5 fg/mL
decolorization immunoassay (this work)	0.05 to 8 ng/mL (1.3×10^{-5} − 2.1×10^{-3} U/mL)	0.02 ng/mL (5.2×10^{-6} U/mL)

An excellent biosensor must have good selectivity to detect the target without any interference accurately. For interference study, the wells were incubated with an $MGNRs_{CA19-9}/MGNRs_{MUC1}$ mixture and typical interferences that mostly

DOI: 10.1021/acsabm.9b00616
ACS Appl. Bio Mater. XXXX, XXX, XXX−XXX

exist in human blood together, including AA, UA, IgG, FBS, BSA, CEA, and VEGF. Our sensing system specifically captured the target proteins (CA19−9 and MUC1) and prevented the nonspecific adsorption of the $MGNRs_{CA19-9}$/$MGNRs_{MUC1}$ mixture on the well surface. The results showed that no obvious decrease of A_{508nm} was observed when the interferences were incubated with the $MGNRs_{CA19-9}$/$MGNRs_{MUC1}$ and wells in the presence of $NaBH_4$, compared with the PBS group. By contrast, a significant decrease of A_{508nm} was observed when CA19−9 (8.8×10^{-3} U/mL) or MUC1 (1.3×10^{-3} U/mL) was added for incubation with the $MGNRs_{CA19-9}$/$MGNRs_{MUC1}$ and wells in the presence of $NaBH_4$ (Figure 4C), indicating the $MGNRs_{CA19-9}$/$MGNRs_{MUC1}$ would only bind onto the plate well in the presence of CA19−9 or MUC1 and not nonspecifically adsorbed on the well surface. As a result, we confirmed that our decolorization-based immunosensing system could be used for highly sensitive, selective, and accurate CA19−9 and MUC1 detection.

3.6. Specificity of CA19−9 and MUC1 Proteins in Spiked Serum Sample. To prove the accuracy of our immunosensing system for CA19−9 and MUC1 detection, various concentrations of CA19−9 or MUC1 were spiked into human serum, ranging from 0.75 ng/mL (1.296×10^{-3} U/mL for CA19−9; 1.935×10^{-4} U/mL for MUC1) to 5 ng/mL (8.640×10^{-3} U/mL for CA19−9; 1.290×10^{-3} U/mL for MUC1), and the ΔA_{508nm} nm was recorded to measure the concentrations of added CA19−9 or MUC1; the results are showed in Table 3. The recovery rates of CA19−9 and MUC1

Table 3. Determination of Spiked CA19-9 and MUC1 in Serum Samples Using the Immunosensor with MGNRs

sample	spiked (ng/mL)/(U/mL)	detected (ng/mL)/(U/mL)	recovery (%)	RSD (n = 3, %)
initial CA19−9 in serum	0	$0.154/2.661 \times 10^{-4}$		
1	$0.75/1.296 \times 10^{-3}$	$0.894/1.544 \times 10^{-3}$	98.90	3.19
2	$1.25/2.160 \times 10^{-3}$	$1.455/2.514 \times 10^{-3}$	104.08	5.94
3	$5/8.640 \times 10^{-3}$	$5.401/9.317 \times 10^{-3}$	104.94	0.42
initial MUC1 in serum	0	$0.114/2.941 \times 10^{-5}$		
1	$0.75/1.935 \times 10^{-4}$	$0.895/2.309 \times 10^{-4}$	104.13	3.19
2	$1.25/3.225 \times 10^{-4}$	$1.36/3.509 \times 10^{-4}$	99.72	5.03
3	$5/1.290 \times 10^{-3}$	$5.365/1.384 \times 10^{-3}$	105.02	1.61

were acceptable (98.9−105.02%), and the relative standard deviation was lower than 6.0%, indicating that our immunosensing system is accurate enough for CA19−9 and MUC1 detection. As a result, we confirmed that our immunosensing system based on MGNRs for the decolorization of MO could be used for highly sensitive, selective, and accurate CA19−9 and MUC1 detection.

4. CONCLUSION

In this study, we have successfully developed an $MGNRs_{CA19-9}$/$MGNRs_{MUC1}$ mixture with high sensitivity, stability, selectivity, and catalytic activity to reduce MO as a signal probe, forming an ultrasensitive immunosensor with an antibody-coating plate well for simple and rapid diagnosis and prognosis monitoring of PC. As a result of this approach, we demonstrated that this enzyme-free colorimetric immunosensor can be used for accurate detection of CA19−9 and MUC1 in serum as well as an ELISA assay can, and it can also widen the detection range of CA19−9 and MUC1 from 8.6×10^{-5} U/mL to 1.4×10^{-2} U/mL for CA19−9 with a LOD of 3.5×10^{-5} U/mL and 1.3×10^{-5} U/mL to 2.1×10^{-3} U/mL for MUC1 with a LOD of 5.2×10^{-6} U/mL, which was achieved within 60 min, allowing for the detection of CA19−9 and MUC1 in clinical human serum samples for PC diagnosis and prognosis monitoring in the future.

■ ASSOCIATED CONTENT

Supporting Information

The Supporting Information is available free of charge on the ACS Publications website at DOI: 10.1021/acsabm.9b00616.

Histogram of the surface ζ potential in the fabrication process of MGNRs, UV−vis absorption spectra of MO with different structured forms at equal concentration, and line graph of the stability of MGNRs stored at 25, 37, and 50 °C for a period of 1−90 days (PDF)

■ AUTHOR INFORMATION

Corresponding Author

*Tel: (+886)-7-5252000 ext. 5842. E-mail: howardyang@mail.nsysu.edu.tw.

ORCID

Nan-Si Li: 0000-0002-6991-6223

Hung-Wei Yang: 0000-0002-8438-6291

Author Contributions

#N.-S.L. and W.-L.L. contributed equally to this work.

Notes

The authors declare no competing financial interest.

■ ACKNOWLEDGMENTS

This work was financially supported by the Kaohsiung Armed Forces General Hospital (108-32) and Ministry of Science and Technology (MOST106-2628-E-110-001-MY3, MOST106-2628-B-110-001-MY4), Taiwan, R.O.C. We would also like to thank the Chang Gung Memorial Hospital Microscopy Core Laboratory for their assistance with TEM.

■ REFERENCES

(1) Siegel, R. L.; Miller, K. D.; Jemal, A. Cancer statistics, 2016. *Ca-Cancer J. Clin.* **2016**, *66* (1), 7−30.

(2) Goonetilleke, K. S.; Siriwardena, A. K. Systematic review of carbohydrate antigen (CA 19−9) as a biochemical marker in the diagnosis of pancreatic cancer. *Eur. J. Surg. Oncol.* **2007**, *33* (3), 266−270.

(3) Gold, D. V.; Karanjawala, Z.; Modrak, D. E.; Goldenberg, D. M.; Hruban, R. H. PAM4-reactive MUC1 is a biomarker for early pancreatic adenocarcinoma. *Clin. Cancer Res.* **2007**, *13* (24), 7380−7387.

(4) Gold, D. V.; Goggins, M.; Modrak, D. E.; Newsome, G.; Liu, M.; Shi, C.; Hruban, R. H.; Goldenberg, D. M. Detection of early-stage pancreatic adenocarcinoma. *Cancer Epidemiol., Biomarkers Prev.* **2010**, *19* (11), 2786−2794.

(5) Roy, L. D.; Sahraei, M.; Subramani, D. B.; Besmer, D.; Nath, S.; Tinder, T. L.; Bajaj, E.; Shanmugam, K.; Lee, Y. Y.; Hwang, S. I.; et al. MUC1 enhances invasiveness of pancreatic cancer cells by inducing epithelial to mesenchymal transition. *Oncogene* **2011**, *30* (12), 1449−1459.

DOI: 10.1021/acsabm.9b00616
ACS Appl. Bio Mater. XXXX, XXX, XXX−XXX

(6) Ambrosi, A.; Airo, F.; Merkoci, A. Enhanced gold nanoparticle based ELISA for a breast cancer biomarker. *Anal. Chem.* **2010**, *82* (3), 1151−1156.
(7) Zhang, A.; Xiang, H.; Zhang, X.; Guo, W.; Yuan, E.; Huang, C.; Jia, N. A novel sandwich electrochemiluminescence immunosensor for ultrasensitive detection of carbohydrate antigen 19−9 based on immobilizing luminol on Ag@BSA core/shell microspheres. *Biosens. Bioelectron.* **2016**, *75*, 206−212.
(8) Sha, Y.; Guo, Z.; Chen, B.; Wang, S.; Ge, G.; Qiu, B.; Jiang, X. A one-step electrochemiluminescence immunosensor preparation for ultrasensitive detection of carbohydrate antigen 19−9 based on multi-functionalized graphene oxide. *Biosens. Bioelectron.* **2015**, *66*, 468−473.
(9) Jiang, X.; Wang, H.; Yuan, R.; Chai, Y. Sensitive electrochemiluminescence detection for CA15−3 based on immobilizing luminol on dendrimer functionalized ZnO nanorods. *Biosens. Bioelectron.* **2015**, *63*, 33−38.
(10) Khan, M. M.; Lee, J.; Cho, M. H. Au@TiO_2 nanocomposites for the catalytic degradation of methyl orange and methylene blue: an electron relay effect. *J. Ind. Eng. Chem.* **2014**, *20* (4), 1584−1590.
(11) Nikoobakht, B.; El-Sayed, M. A. Preparation and Growth Mechanism of Gold Nanorods (NRs) Using Seed-Mediated Growth Method. *Chem. Mater.* **2003**, *15* (10), 1957−1962.
(12) Wang, C.; Irudayaraj, J. Gold Nanorod Probes for the Detection of Multiple Pathogens. *Small* **2008**, *4* (12), 2204−2208.
(13) Yang, H. W.; Liu, H. L.; Li, M. L.; Hsi, I. W.; Fan, C. T.; Huang, C. Y.; Lu, Y. J.; Hua, M. Y.; Chou, H. Y.; Liaw, J. W.; et al. Magnetic gold-nanorod/PNIPAAmMA nanoparticles for dual magnetic resonance and photoacoustic imaging and targeted photothermal therapy. *Biomaterials* **2013**, *34* (22), 5651−5660.
(14) Peng, C.; Hua, M. Y.; Li, N. S.; Hsu, Y. P.; Chen, Y. T.; Chuang, C. K.; Pang, S. T.; Yang, H. W. A colorimetric immunosensor based on self-linkable dual-nanozyme for ultrasensitive bladder cancer diagnosis and prognosis monitoring. *Biosens. Bioelectron.* **2019**, *126*, 581−589.
(15) Zhang, H.; Sun, Y.; Gao, S.; Zhang, H.; Zhang, J.; Bai, Y.; Song, D. Studies of gold nanorod-iron oxide nanohybrids for immunoassay based on SPR biosensor. *Talanta* **2014**, *125*, 29−35.
(16) Pan, L. H.; Pang, S. T.; Fang, P. Y.; Chuang, C. K.; Yang, H. W. Label-free biochips for accurate detection of Prostate Cancer in clinic: Dual biomarkers and circulating tumor cells. *Theranostics* **2017**, *7* (17), 4289−4300.
(17) Huang, H.; He, C.; Zeng, Y.; Xia, X.; Yu, X.; Yi, P.; Chen, Z. A novel label-free multi-throughput optical biosensor based on localized surface plasmon resonance. *Biosens. Bioelectron.* **2009**, *24* (7), 2255−2259.
(18) Li, Z.; Qiang, L.; Zhong, S.; Wang, H.; Cui, X. Synthesis and characterization of monodisperse magnetic Fe_3O_4@BSA core−shell nanoparticles. *Colloids Surf., A* **2013**, *436*, 1145−1151.
(19) Su, G.; Yang, C.; Zhu, J. J. Fabrication of gold nanorods with tunable longitudinal surface plasmon resonance peaks by reductive dopamine. *Langmuir* **2015**, *31* (2), 817−823.
(20) Newati, S. J.; Singh, V. M.; Sachdeva, S.; Khan, R. A. Iron oxide nanoparticles reinforced self-assembled monolayer of cysteamine for use in enzymatic biosensor development. *Nano Sci. Technol. Inst* **2010**, *3*, 39−42.
(21) Song, J. Y.; Jang, H. K.; Kim, B. S. Biological synthesis of gold nanoparticles using Magnolia kobus and Diopyros kaki leaf extracts. *Process Biochem.* **2009**, *44* (10), 1133−1138.
(22) Gupta, N.; Singh, H. P.; Sharma, R. K. Metal nanoparticles with high catalytic activity in degradation of methyl orange: an electron relay effect. *J. Mol. Catal. A: Chem.* **2011**, *335* (1−2), 248−252.
(23) Li, L.; Yin, D.; Xu, K.; Liu, Y.; Song, D.; Wang, J.; Zhao, C.; Song, X.; Li, J. A sandwich immunoassay for brucellosis diagnosis based on immune magnetic beads and quantum dots. *J. Pharm. Biomed. Anal.* **2017**, *141*, 79−86.
(24) Gao, L.; Zhuang, J.; Nie, L.; Zhang, J.; Zhang, Y.; Gu, N.; Wang, T.; Feng, J.; Yang, D.; Perrett, S.; et al. Intrinsic peroxidase-like activity of ferromagnetic nanoparticles. *Nat. Nanotechnol.* **2007**, *2* (9), 577−583.
(25) Houas, A.; Lachheb, H.; Ksibi, M.; Elaloui, E.; Guillard, C.; Herrmann, J. M. Photocatalytic degradation pathway of methylene blue in water. *Appl. Catal., B* **2001**, *31* (2), 145−157.
(26) Boily, J. F.; Seward, T. M. On the Dissociation of Methyl Orange: Spectrophotometric Investigation in Aqueous Solutions from 10 to 90°C and Theoretical Evidence for Intramolecular Dihydrogen Bonding. *J. Solution Chem.* **2005**, *34* (12), 1387−1406.
(27) Duffy, M. J.; Sturgeon, C.; Lamerz, R.; Haglund, C.; Holubec, V. L.; Klapdor, R.; Nicolini, A.; Topolcan, O.; Heinemann, V. Tumor markers in pancreatic cancer: a European Group on Tumor Markers (EGTM) status report. *Ann. Oncol.* **2010**, *21* (3), 441−7.
(28) Gold, D. V.; Modrak, D. E.; Ying, Z.; Cardillo, T. M.; Sharkey, R. M.; Goldenberg, D. M. New MUC1 Serum Immunoassay Differentiates Pancreatic Cancer From Pancreatitis. *J. Clin. Oncol.* **2006**, *24* (2), 252−258.
(29) Guo, A.; Li, Y.; Cao, W.; Meng, X.; Wu, D.; Wei, Q.; Du, B. An electrochemical immunosensor for ultrasensitive detection of carbohydrate antigen 199 based on Au@ CuxOS yolk−shell nanostructures with porous shells as labels. *Biosens. Bioelectron.* **2015**, *63*, 39−46.
(30) Jawad, Z. A.; Theodorou, I. G.; Jiao, L. R.; Xie, F. Highly sensitive plasmonic detection of the pancreatic cancer biomarker CA 19−9. *Sci. Rep.* **2017**, *7* (1), 14309.
(31) Zhang, A.; Xiang, H.; Zhang, X.; Guo, W.; Yuan, E.; Huang, C.; Jia, N. A novel sandwich electrochemiluminescence immunosensor for ultrasensitive detection of carbohydrate antigen 19−9 based on immobilizing luminol on Ag@ BSA core/shell microspheres. *Biosens. Bioelectron.* **2016**, *75*, 206−212.
(32) Hu, R.; Wen, W.; Wang, Q.; Xiong, H.; Zhang, X.; Gu, H.; Wang, S. Novel electrochemical aptamer biosensor based on an enzyme−gold nanoparticle dual label for the ultrasensitive detection of epithelial tumour marker MUC1. *Biosens. Bioelectron.* **2014**, *53*, 384−389.
(33) He, Y.; Lin, Y.; Tang, H.; Pang, D. A graphene oxide-based fluorescent aptasensor for the turn-on detection of epithelial tumor marker mucin 1. *Nanoscale* **2012**, *4* (6), 2054−2059.
(34) Wang, J. X.; Zhuo, Y.; Zhou, Y.; Yuan, R.; Chai, Y. Q. Electrochemiluminescence immunosensor based on multifunctional luminol-capped AuNPs@ Fe_3O_4 nanocomposite for the detection of mucin-1. *Biosens. Bioelectron.* **2015**, *71*, 407−413.

DOI: 10.1021/acsabm.9b00616
ACS Appl. Bio Mater. XXXX, XXX, XXX−XXX